Applied Surface Science 354 (2015) 437–442

Contents lists available at ScienceDirect

Applied Surface Science

journal homepage: www.elsevier.com/locate/apsusc

Hybrid functional calculated optical and electronic structures of thin anatase TiO_2 nanowires with organic dye adsorbates

Hatice Ünal[a], Deniz Gunceler[b], Oğuz Gülseren[c], Şinasi Ellialtıoğlu[d], Ersen Mete[a,*]

[a] Department of Physics, Balıkesir University, Balıkesir 10145, Turkey
[b] Department of Physics, Cornell University, Ithaca, NY 14853, USA
[c] Department of Physics, Bilkent University, Ankara 06800, Turkey
[d] Basic Sciences, TED University, Ankara 06420, Turkey

ARTICLE INFO

Article history:
Received 25 December 2014
Received in revised form 10 April 2015
Accepted 11 April 2015
Available online 20 April 2015

ABSTRACT

The electronic and optical properties of thin anatase TiO_2 (1 0 1) and (0 0 1) nanowires have been investigated using the screened Coulomb hybrid density functional calculations. For the bare nanowires with sub-nanometer diameters, the calculated band gaps are larger relative to the bulk values due to size effects. The role of organic light harvesting sensitizers on the absorption characteristics of the anatase nanowires has been examined using the hybrid density functional method incorporating partial exact exchange with range separation. For the lowest lying excitations, directional charge redistribution of tetrahydroquinoline (C2-1) dye shows a remarkably different profile in comparison to a simple molecule which is chosen as the coumarin skeleton. The binding modes and the adsorption energies of C2-1 dye and coumarin core on the anatase nanowires have been studied including non-linear solvation effetcs. The calculated optical and electronic properties of the nanowires with these two different types of sensitizers have been interpreted in terms of their electron–hole generation, charge carrier injection and recombination characteristics.

1. Introduction

The wide-bandgap semiconductor titanium dioxide (TiO_2) has attracted attention since the discovery of its remarkable photocatalytic activity under UV irradiation [1,2]. TiO_2 can be functionalized for operation under visible light illumination by impurity dopants or by sensitizing molecular adsorbates. The latter is particularly important in dye sensitized solar cell (DSSC) applications where nanoporous TiO_2 film is used as the anode electrode [3]. Titania surfaces offer good adsorption characteristics and can easily be covered with a monolayer of a light harvesting dye. The operational system sits in an organic solvent electrolyte with a redox system like iodide/triiodide couple. Photo excitation of the molecule leads to electron–hole generation and subsequent charge injection to the conduction band (CB) of the oxide which acts as a current collector. Then, an electron is donated from the electrolyte to restore the ground state of the dye. On the other hand, the charge carrier transfer throughput is limited due to recombination rate. Therefore, the surface area of the oxide and the choice of the dye becomes important in the overall cell efficiency.

The crystal structures of titania occur mainly in anatase, rutile and brookite phases in nature. Under ambient conditions and in its bulk form, rutile is the most stable polymorph. The optical gaps are measured as ~3.2 eV for anatase [4] and as ~3.0 eV for rutile [5]. The anatase phase especially its (0 0 1) surface is known to exhibit higher photocatalytic activity in many situations [6]. Moreover, TiO_2 nanomaterials with grain sizes smaller than 14 nm are found to be in anatase form rather than in rutile structure [7,8]. Electronically, thin anatase nanowires exhibit different features relative to other nanoparticulate titania electrodes. In particular, the increase in the corresponding band gaps and photocatalytic oxidation powers become more apparent as the nanowire diameters tend to be smaller than 2 nm due to the confinement effect [9–11].

The progress in the synthesis of quasi-one-dimensional oxide nanostructures opens up new possibilities to fabricate technologically attractive applications. Recently, titania nanowires and nanorods become candidate building blocks of highly ordered architectures for solar cells [12]. They offer large surface-to-volume ratios which also enhance *n*-type conductivity properties [13–15]. In addition, this is seen as an important factor in reducing the charge carrier recombination rates. Therefore, the use of quasi-one-dimensional titania as the current collector component is a promising way to improve cell efficiencies.

* Corresponding author. Tel.: +90 5335733595.
E-mail address: emete@balikesir.edu.tr (E. Mete).

http://dx.doi.org/10.1016/j.apsusc.2015.04.086
0169-4332/

Organic photosensitizers have become a good alternative to metal driven commercial dyes not only because they are cheap, environmentally friendly and easy to isolate but also because their electronic and anchoring characteristics can be modified through variously functional attachable moieties. Recently, a class of novel organic sensitizers based on tetrahydroquinoline moiety as the electron donor group have been proposed to achieve photoinduced intramolecular charge transfer [16]. For instance, π-conjugated electron donor acceptor (D-π-A) type C2-1 dye has the highest conversion efficiency of 4.5% within this family [17].

Theoretical prediction of molecular and material properties have been focused by many researchers to understand and improve functional dye sensitizers adsorbed on the oxide [18–24]. Tetrahydroquinoline based D-π-A type dyes on TiO_2(1 0 1) surface have been studied using standard density functional slab calculations where two-dimensional periodicity was adopted [25,26]. In this work, we examined the band gap features of thin anatase (1 0 1) and (0 0 1) nanowire models using the range separated hybrid density functional theory calculations. Then, we considered isolated C2-1 ($C_{21}H_{20}N_2SO_2$) charge transfer dye on these nanowires for their adsorption geometries and their binding energies in the solution using a nonlinear solvation model. We have also investigated the electronic properties of the resulting combined physical system such as the densities of states, the charge densities of the frontier states and the absorption spectra. In order to make a comparison with a simple skeleton molecule, we have chosen the coumarin core ($C_9H_6O_2$) and repeated the same computations systematically for the coumarin on the thin anatase (0 0 1) and (1 0 1) nanowires using the hybrid method beyond the standard DFT. In fact, coumarin dyes with various anchoring groups has been extensively studied in the literature by theoretical works [27–39,41,40,42,43].

2. Computational details

We performed periodic total energy density functional theory calculations using the implementation of the screened Coulomb hybrid exchange-correlation scheme, HSE [44–46], in the Vienna ab-initio simulation package (VASP) [47]. Single particle states were expanded in terms of plane waves up to a kinetic energy cutoff of 400 eV using the projector-augmented waves (PAW) method [48,49]. Brillouin zone integrations were carried out over a k-point sampling to get well-converged values.

The standard DFT exchange-correlation functionals like PBE [51] suffers from the lack of proper self-interaction cancellation (SIC) as in the Hartree–Fock approximation to the interacting many particle problem. In general, in the hybrid approaches, the nonlocal exact exchange energy is partially admixed with the semilocal PBE exchange energy in order to improve the description of the localized states such as the d-orbitals of the TiO_2. Since, the bottom of the conduction band (CB) of titania is composed of 3d-states having t_{2g} symmetry, hybrid DFT methods significantly heal the band gap underestimation of the standard exchange-correlation schemes.

The range separated hybrid HSE functional treats the exchange energy as composed of long-range (LR) and short-range (SR) parts,

$$E_{\mathbf{X}}^{\mathrm{HSE}} = aE_{\mathbf{X}}^{\mathrm{HF,SR}}(\omega) + (1-a)E_{\mathbf{X}}^{\mathrm{PBE,SR}}(\omega) + E_{\mathbf{X}}^{\mathrm{PBE,LR}}(\omega)$$

where a is the mixing factor [50] and ω is the range separation parameter [44–46]. The correlation energy is taken from standard PBE correlation energy [51]. In our calculations we used a mixing factor of a = 0.22 to reproduce the experimental bulk band gap of anatase as 3.20 eV.

Solvation effects have been included at the hybrid HSE exchange-correlation functional level for C2-1 and coumarin on the anatase nanowires considered in this work. We performed calculations for chloroform and water environment via polarizable continuum model (PCM) including both the new non-linear and its linear counterpart as implemented in the open-source code JDFTx [52–55]. The solvent environment is reproduced by a dielectric medium surrounding the solute dye molecule. The dielectric function of the solute turns on around a critical density value which

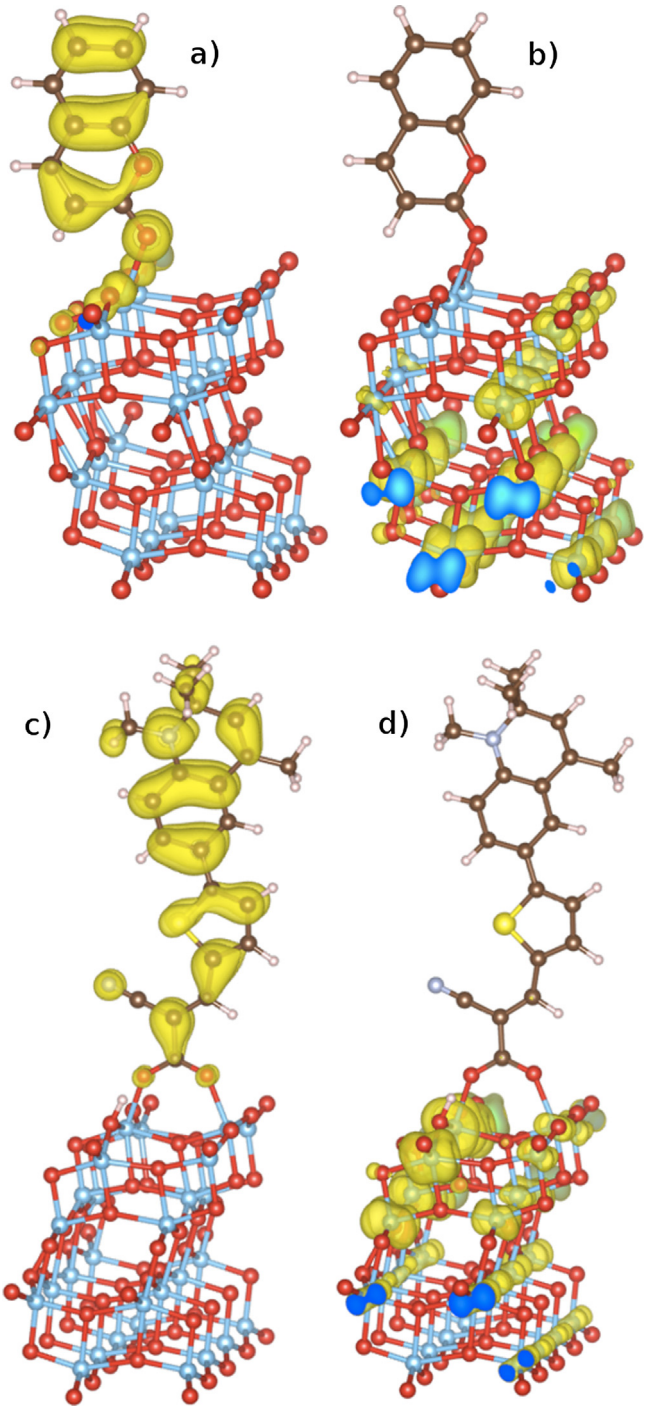

Fig. 1. The charge density distribution plots of the highest occupied states of coumarin+001nw (a), C2-1+001nw (c), and of the lowest unoccupied states of coumarin+001nw (b), C2-1+001nw (d) calculated using the HSE functional. In this ball-stick representation, the red, light-blue, brown, grey, yellow and white colors are used for O, Ti, C, N, S and H atoms, respectively. (For interpretation of the references to color in this figure legend, the reader is referred to the web version of the article.)

is used to model the cavity around the solute and parametrized to reproduce experimental solvation energies [53,54].

The anatase 001nw and 101nw model structures are cleaved from the bulk phase as shown in Figs. 1 and 2. Both nanowires with and without C2-1 and coumarin molecules are considered in large periodic tetragonal supercells. The nanowires have periodicity in one dimension. A vacuum separation of at least 20 Å is adopted around the nanowire in order to avoid any unphysical interaction with its periodic images in the directions perpendicular to the nanowire axis. We also used larger periodicity along the nanowire axis in order to consider the dye molecules as isolated on the (0 0 1) and (1 0 1) facets. We constructed several probable initial adsorption geometries. The atomic positions were fully optimized using the conjugate-gradients algorithm by minimizing the Hellmann–Feynman forces on each atom until a threshold value of 0.01 eV/Å is reached to stop the self-consistent cycles. The relaxed nanowire models keep the anatase form without a major structural distortion [56].

We calculated the absorption spectra by considering the transitions from the occupied to the unoccupied states within the first Brillouin zone [57]. The imaginary part of the frequency dependent dielectric function $\varepsilon_2(\omega)$ can be expanded as a sum over single particle states determined by the self-consistent HSE calculations.

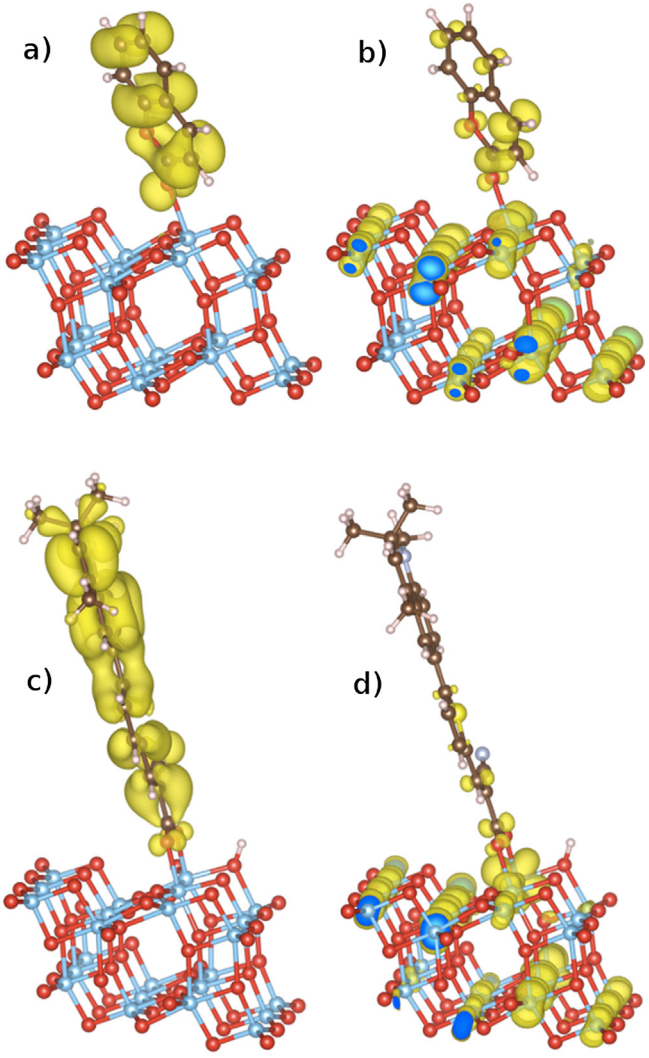

Fig. 2. The charge density distribution plots of the highest occupied states of coumarin+101nw (a), C2-1+101nw (c), and of the lowest unoccupied states of coumarin+101nw (b), C2-1+101nw (d) calculated using the HSE functional.

3. Results and discussion

Thin 001nw and 101nw models have been considered in periodic supercells with large vacuum separations. Their atomic positions have been relaxed using the HSE exchange-correlation functional. We did not fix any of the ionic cores to their bulk positions in any of the geometry optimization calculations in this work. Although the HSE-optimized atomic structures of the bare nanowires are not shown, they did not have any major reconstruction from their initial geometries similar to those obtained previously [56]. The surface Ti—O bond lengths become slightly larger than the bulk value of 1.95 Å. This difference gets much smaller toward the center of the nanowires. Therefore, both 001nw and 101nw models maintain the anatase structure.

We have considered a number of probable initial adsorption configurations for C2-1 molecule on both of the nanowire models. The tail oxygen and the OH group are found to be actively involved in the adsorption of the dye on the oxide surface (see Figs. 1 and 2). C2-1 molecule can achieve relatively high adsorption energies in its bidentate mode as presented in Table 1. In this case, the OH group loses its hydrogen to one of the nearby surface oxygens and the remaining two tail oxygens form two Ti—O bonds with the anatase surface. In the monodentate binding, however, C2-1 forms only one Ti—O bond through its tail oxygen. The bidentate dye-surface bond lengths are ~2.0 Å which is close to the bulk value. C2-1 molecule slightly distorts the nanowire structure only locally.

As a reference minimal skeleton, we considered the coumarin core on the nanowire surfaces. In this case, coumarin prefers to form a single bond with a 5-fold coordinated surface Ti atom by aligning perpendicular to both of the nanowires as an energetically favorable binding configuration. The Ti—O bonds between the dye and the surface become 2.18 Å and 2.21 Å on 101nw and 001nw, respectively. The distortion of coumarin on the nanowire structure is even smaller relative to the C2-1 case.

The C2-1 complex is known to have photoinduced intramolecular charge transfer in the gas phase. On the other hand, both the HOMO and the LUMO charge densities remain localized on the entire coumarin core. Therefore, their charge redistributions are remarkably different if they are considered to be isolated. Their charge density relocation characteristics upon an excitation becomes important when these molecules are attached to an oxide surface. In order to interpret the charge injection features of these two different dyes we calculated the charge densities of highest occupied and lowest unoccupied states of dye + nw combined systems. Our HSE results are depicted in Fig. 1 for 001nw and in Fig. 2 for 101nw cases. The donor-to-acceptor character of C2-1 dye, which can be explained as the intramolecular charge transfer from the tetrahydroquinoline moiety to the π-conjugated acidic part, is significantly modified when the molecule is adsorbed on the titania surfaces. The charge density of the highest occupied state of the combined system is distributed over the entire molecule similar to the case of coumarin on the nanowires. Similar behavior is seen on both 001nw and 101w. However, the charge density distributions of the lowest lying unoccupied states of C2-1+001nw and coumarin+001nw are remarkably different. This can be clearly seen by comparing the corresponding charge density plots in Fig. 1b and d. In the case of 101nw, both dyes exhibit similar charge redistribution features between the highest occupied and the lowest unoccupied states.

The binding energies of C2-1 and coumarin on the 001nw and 101nw for monodentate and bidentate adsorption modes are calculated at the HSE level by the standard formulation used in similar systems previously [18,19]. Moreover, we included solvation effects for the chloroform and water environments using HSE functional and a new nonlinear PCM. Our HSE + PCM results are presented in Table 1. Monodentate bonding of coumarin and C2-1

Table 1
Calculated adsorption energies of dye molecules on thin anatase (0 0 1) and (1 0 1) nanowire structures in vacuum and in solution using HSE method and nonlinear PCM. Energy values are given in eV.

Dye	@001nw			@101nw		
	HSE	HSE+PCM ($CHCl_3$)	HSE+PCM (H_2O)	HSE	HSE + PCM ($CHCl_3$)	HSE + PCM (H_2O)
Coumarin	−0.63	−0.33	−0.07	−0.70	−0.58	−0.44
C2-1(monodentate)	−0.73	−0.65	−0.11	−0.62	−0.43	−0.30
C2-1(bidentate)	−1.25	−1.18	−0.52	−0.83	−0.70	−0.51

on both (0 0 1 and (1 0 1) surfaces show similarly moderate adsorption energies in vacuum and also in the solution. Single bonds are found to be drastically weakened by the dielectric environment of the strong solutions like water. Therefore, these type of monodentate binding modes are not expected to be durable and stable in the electrolyte environment. On the other hand, bidentate mode of C2-1 on the oxide surfaces gives reasonably strong binding energies. Therefore, C2-1 dye forming two O-Ti bonds with the surface can even be stable in an ionic solvent like water. These HSE + PCM results show the significance of anchoring of the light harvesting sensitizers for a reliable DSSC operation.

The inclusion of the nonlinear PCM changes the binding energies in the positive direction. The main reason is that the dye molecule and the adsorption sites on the TiO_2 surface interact with the solvent very strongly. Because such an interaction is not present in vacuum calculations, results give more negative binding energies. Since water is a more polar solvent than chloroform, it has a higher dielectric constant. Hence, water interacts more strongly with the adsorption sites. Therefore calculated binding energies in H_2O are more positive than those in $CHCl_3$.

The geometry optimization by minimizing the Hellmann–Feynman forces causes surface ionic cores to relax into their minimum energy positions. Hence, possible surface states are passivated yielding a clean band gap (Fig. 3). The HSE method gave the band gaps of bare nanowires as 4.06 eV for 001nw and 4.01 eV for 001nw. These are significantly larger than both HSE-calculated and experimentally measured bulk value of 3.20 eV. For the nanowire diameters around 1 nm, HSE calculations indicate a strong quantum confinement effect [56]. This widening of the gap, upon adsorption of dyes, results in some molecular states to fall into the energy gap, where most of the deeper lying occupied molecular orbitals stay in the valence band as resonant states. Consequently, the Fermi energy shifts up to higher energies leading to an energy-gap narrowing which is an important factor for photovoltaic properties. On the other hand, the lowest lying unoccupied molecular levels of the dyes delocalize on the Ti 3*d* states inside the conduction band (CB) of the nanowires, as channels of excited electron injection to the nanowires. The density of states (DOS) of the combined dye + nanowire systems have also been presented in Fig. 3 for coumarin, and C2-1 in two modes, namely mono- and bidentate forms. For both of the nanowires, the molecular states of coumarin appear around the VB edge while one of them is isolated from the rest. For C2-1 monodentate mode, essentially three filled isolated states fall into the band gap of both nanowire types. On going from monodentate to bidentate bonding, an additional isolated state appears above the VB. Significant band gap reduction is obtained in the case of C2-1 bridging in bidentate form on both types of nanowires, which makes C2-1 dye with such bonding more important for light harvesting.

As we discussed with the electronic structure, appearance of several new dye related states within the band gap of nanowires might cause a redshift of the optical absorption of these dye-nanowire composite systems if the transitions from these states are symmetry allowed, so they might become active in the visible part of the spectrum which is very beneficiary for photovoltaic applications. In order to investigate the optical absorption, we have calculated the dipole matrix elements between occupied and empty states for each case, which is essentially the imaginary part of the dielectric function, $\epsilon_2(\omega)$. The calculated absorption spectra for clean anatase nanowire along with those for the corresponding dye-nanowire composite systems are depicted in Fig. 4(a) and (b) for (0 0 1) and (1 0 1) nanowires, respectively. First of all, when we compare the corresponding optical absorption spectra of the different nanowire and nw+dye systems, general features are very

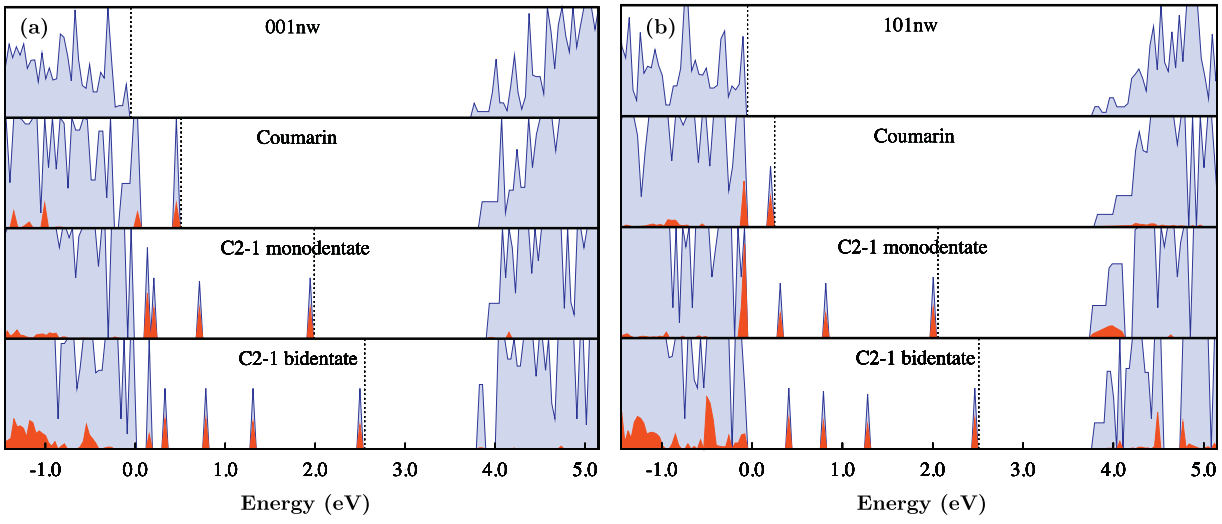

Fig. 3. The HSE-calculated partial and total densities of states (DOS) of (C2-1,coumarin)+nanowire combined systems for low energy binding modes. The results are shown for 001nw on the left and for 101nw on the right panes. The molecular contributions are indicated as dark(red) shades.The dotted lines denote the Fermi energies and set at slightly above the highest occupied states. The DOS structures are aligned with respect to the valence band maximum of the bare cases for each type of nanowires. (For interpretation of the references to color in this figure legend, the reader is referred to the web version of the article.)

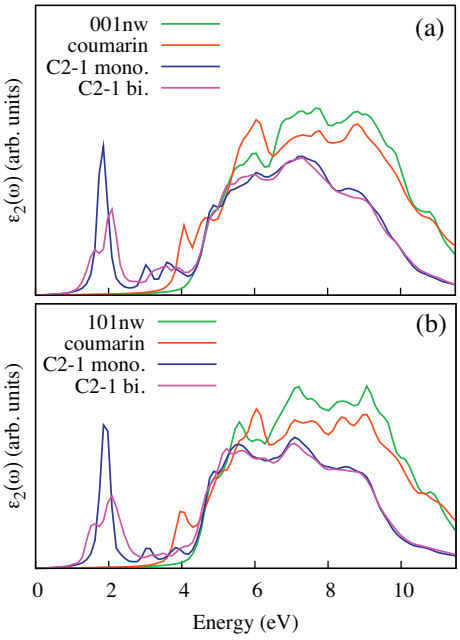

Fig. 4. Absorption spectra of bare and dye adsorbed 001nw (a) and 101nw (b) cases calculated using the HSE hybrid DFT method.

similar for both (0 0 1) and (1 0 1) nanowires. For bare nanowires, the absorption starts after 4 eV, which coincides with energy band gap of the nanowire, therefore we can say that the absorption edge is from the valence band edge to the conduction band edge. However, when coumarin is attached to the nanowire, two new states, one very close the valance band edge and the other is almost 0.8 eV above the edge, associated with the dye appears within the band gap of the nanowire. These are the reason of the two peaks observed near the adsorption edge absorption spectrum of coumarin+nanowire system, otherwise the spectrum looks very similar to the bare nanowire one. In the case of C2-1 dye, there are several dye originates states within the band gap for both of the adsorption modes, monodentate and bidantate. The absorption spectra of both of the modes are similar. Compared to the bare nanowire spectrum, there are two new peaks, one around 2 eV at the middle of the band gap and the other around 3 eV almost 1 eV below the absorption edge (or equivalently conduction band edge). For monodentate mode, the peak at 2 eV is sharp while there are two peaks around 3 eV. However, for bidentate, we have two split peaks around 2 eV, and one very broad peak around 3 eV instead of two peaks of monodentate case. Comparing these peak positions with DOS reported in Fig. 3, we can conclude that the peak around 2 eV is due to a transition from dye associated state at the Fermi level to the conduction band edge. For both dye types the LUMO levels strongly resonate with the CB when they are attached to the surface of the oxide nanowire. Meanwhile, the HOMO-like levels appear in the bandgap of TiO_2 nanowires as isolated and well-localized states on the dye. The associated charge density distributions can also be seen in Fig. 1. Briefly, the lower lying peaks in the absorption spectra for the dye + nw combined systems, are essentially due to the transitions from the dye-related HOMO-like level to the states at the bottom of the conduction band.

4. Conclusions

We have investigated the band gap related properties and resulting absorption spectra of bare thin anatase nanowires with diameters less than 1 nm. We used the range separated hybrid HSE functional within DFT. For these nanowires, the HSE approach estimates reasonably larger band gaps in agreement with the quantum confinement effect. The same level of theory was applied to examine the adsorption configurations, electronic structures and optical profiles of D-π-A type organic C2-1 photosensitizer on the (0 0 1) and (1 0 1) facets of the oxide nanowires. The intramolecular charge transfer character of C2-1 appears to be modified once the C2-1 forms a bidentate bonding with the surface oxygens on the anatase nanowires. The C2-1+nw system shows similar spatial charge density features with that of the coumarin+nw for the highest occupied state which is actively involved in the lowest lying photoexcitation. The HSE + PCM including nonlinear dielectric effects shows that the binding energy of C2-1 dye remains moderate in solution environment. This might be seen as one of the explanations of why the anchoring of sensitizer molecules on the oxide surface is important. The number of dye related states above the VB of the titania nanowires is associated with the complexity of the molecular structure. Therefore, functional moeities are desirable to absorb a larger portion of the visible spectrum. Consequently, the use of range separated hybrid density functionals is a promising way to describe band gap related electronic structures for dye and TiO_2 nanowire systems.

Acknowledgments.

This work is supported by TÜBİTAK, The Scientific and Technological Research Council of Turkey (Grant #110T394). Computational resources were provided by ULAKBİM, Turkish Academic Network & Information Center.

References

[1] A. Fujishima, K. Honda, Nature (London) 238 (1972) 37.
[2] A. Fujishima, X.T. Zhang, D.A. Tryk, Surf. Sci. Rep. 63 (2008) 515.
[3] B. O'Regan, M. Grätzel, Nature 353 (1991) 737.
[4] L. Kavan, M. Grätzel, S.E. Gilbert, C. Klemenz, H.J. Scheel, J. Am. Chem. Soc. 118 (1996) 6716.
[5] J. Pascaul, J. Camassel, H. Mathieu, Phys. Rev. Lett. 39 (1977) 1490.
[6] U. Diebold, Surf. Sci. Rep. 48 (2003) 53.
[7] G. Li, L. Li, J. Boerio-Goates, B.F. Woodfield, J. Am. Chem. Soc. 127 (2005) 8659.
[8] A.S. Barnard, L.A. Curtiss, Nano Lett. 5 (2005) 1261.
[9] M. Jankulovska, T. Berger, T. Lana-Villarreal, R. Gómez, Electrochim. Acta 62 (2012) 172.
[10] L. Yuan, S. Meng, Y. Zhou, Z. Yue, J. Mater. Chem. A 1 (2013) 2552.
[11] T. Berger, T. Lana-Villarreal, D. Monllor-Satoca, R. Gómez, J. Phys. Chem. C 112 (2008) 15920.
[12] D. Çakır, O. Gülseren, Phys. Rev. B 80 (2009) 125424.
[13] P.K. Naicker, P.T. Cummings, H. Zhang, J.F. Banfield, J. Phys. Chem. B 109 (2005) 15243–15249.
[14] A. Iacomino, G. Cantele, F. Trani, D. Ninno, J. Phys. Chem. C 114 (2010) 12389–12400.
[15] V.C. Fuertes, C.F.A. Negre, M.B. Oviedo, F.P. Bonafé, F.Y. Oliva, C.G. Sánchez, J. Phys. Condens. Matter 25 (2013) 115304.
[16] R. Chen, X. Yang, H. Tian, X. Wang, A. Hagfeldt, L. Sun, Chem. Mater. 19 (2007) 4007–4015.
[17] R. Chen, X. Yang, H. Tian, L. Sun, J. Photochem. Photobiol. A: Chem. 189 (2007) 295–300.
[18] D. Çakır, O. Gülseren, E. Mete, Ş Ellialtıoğlu, Phys. Rev. B 80 (2009) 035431.
[19] D. Çakır, O. Gülseren, E. Mete, Ş Ellialtıoğlu, J. Phys. Chem. C 115 (2011) 9220–9226.
[20] W. Stier, O.V. Prezhdo, J. Phys. Chem. B 106 (2002) 8047–8054.
[21] K. Hara, T. Sato, R. Katoh, A. Furube, Y. Ohga, A. Shinpo, S. Suga, K. Sayama, H. Sugihara, H. Arakawa, J. Phys. Chem. B 107 (2003) 597–606.
[22] J. Banuelos Prieto, F. Lopez Arbeloa, V. Martinez Martinez, I. Lopez Arbeloa, Chem. Phys. 296 (2004) 13–22.
[23] L. Campbell, S. Mukamel, J. Chem. Phys. 121 (2004) 12323.
[24] P. Persson, M.J. Lundqvist, R. Ernstorfer, W.A. Goddard III, F. Willig, J. Chem. Theory Comput. 2 (2006) 441–451.
[25] C.-R. Zhang, L. Liu, J.-W. Zhe, N.-Z. Jin, Y. Ma, L.-H. Yuan, M.-L. Zhang, Y.-Z. Wu, Z.-J. Liu, H.-S. Chen, Int. J. Mol. Sci. 14 (2013) 5461–5481.
[26] C. O'Rourke, D.R. Bowler, J. Phys. Chem. C 114 (2010) 20240–20248.
[27] Z.-S. Wang, F.-Y. Li, C.-H. Huang, L. Wang, M. Wei, L.-P. Jin, N.-Q. Li, J. Phys. Chem. B 104 (2000) 9676.
[28] A. Ehret, L. Stuhl, M.T. Spitler, J. Phys. Chem. B 105 (2001) 9960.
[29] Z.-S. Wang, F.-Y. Li, C.-H. Huang, J. Phys. Chem. B 105 (2001) 9210.
[30] P. Wang, S.M. Zakeeruddin, R. Humphry-Baker, J.E. Moser, M. Grätzel, Adv. Mater. 15 (2003) 2101.

[31] P. Wang, S.M. Zakeeruddin, P. Comte, R. Charvet, R. Humphry-Baker, M. Grätzel, J. Phys. Chem. B 107 (2003) 14336.
[32] T. Horiuchi, H. Miura, K. Sumioka, S. Uchida, J. Am. Chem. Soc. 126 (2004) 12218.
[33] T. Kitamura, M. Ikeda, K. Shigaki, T. Inoue, N.A. Anderson, X. Ai, T. Lian, S. Yangagida, Chem. Mater. 16 (2004) 1806.
[34] Z.-S. Wang, K. Sayama, H. Sugihara, J. Phys. Chem. B 109 (2005) 22449.
[35] D.P. Hagberg, T. Edvinsson, T. Marinado, G. Boschloo, A. Hagfeldt, L. Sun, Chem. Commun. 2245 (2006).
[36] S.-L. Li, K.-J. Jiang, K.-F. Shao, L.-M. Yang, Chem. Commun. 2792 (2006).
[37] Y. Chiba, A. Islam, Y. Watanabe, R. Komiya, N. Koide, L. Han, Jpn. J. Appl. Phys. 45 (2006) L638.
[38] Z.-S. Wang, Y. Cui, K. Hara, Y. Dan-oh, C. Kasada, A. Shinpo, Adv. Mater. 19 (2007) 1138–1141.
[39] Y. Kurashige, T. Nakajima, S. Kurashige, K. Hirao, J. Phys. Chem. A 111 (2007) 5544–5548.
[40] J. Preat, P.-F. Loos, X. Assfeld, D. Jacquemin, E.A. Perpëte, J. Mol. Struct. Theochem. 808 (2007) 85–91.
[41] X. Zhang, J.-J. Zhang, Y.-Y. Xia, J. Photochem. Photobiol. A: Chem. 194 (2008) 167–172.
[42] R. Sanchez-de-Armas, M.A. San Miguel, J. Oviedo, J.F. Sanz, Phys. Chem. Chem. Phys. 14 (2012) 225–233.
[43] C.I. Oprea, P. Panait, F. Cimpoesu, M. Ferbinteanu, M.A. Girtu, Materials 6 (2013) 2372–2392.
[44] J. Heyd, G.E. Scuseria, M. Ernzerhof, J. Chem. Phys. 118 (2003) 8207.
[45] J. Heyd, G.E. Scuseria, M. Ernzerhof, J. Chem. Phys. 124 (2006) 219906.
[46] J. Paier, M. Marsman, K. Hummer, G. Kress, I.C. Gerber, J.G. Angyan, J. Chem. Phys. 125 (2006) 249901.
[47] G. Kresse, J. Hafner, Phys. Rev. B 47 (1993) 558.
[48] P.E. Blöchl, Phys. Rev. B 50 (1994) 17953.
[49] G. Kresse, J. Joubert, Phys. Rev. B 59 (1999) 1758.
[50] J.P. Perdew, M. Ernzerhof, K. Burke, J. Chem. Phys. 105 (1996) 9982.
[51] J.P. Perdew, K. Burke, M. Ernzerhof, Phys. Rev. Lett. 77 (1996) 3865.
[52] K. Letchworth-Weaver, T.A. Arias, Phys. Rev. B 86 (2012) 075140.
[53] D. Gunceler, K. Letchworth-Weaver, R. Sundararaman, K.A. Schwarz, T.A. Arias, Model. Simul. Mater. Sci. Eng. 21 (2013) 074005.
[54] D. Gunceler, T.A. Arias, preprint available at arXiv:1403.6465.
[55] R. Sundararaman, D. Gunceler, K. Letchworth-Weaver, T.A. Arias, JDFTx, 2012 http://jdftx.sourceforge.net
[56] H. Ünal, O. Gülseren, Ş Ellialtıoğlu, E. Mete, Phys. Rev. B 89 (2014) 205127.
[57] M. Gajdoš, K. Hummer, G. Kresse, J. Furthmüller, F. Bechstedt, Phys. Rev. B 73 (2006) 045112.